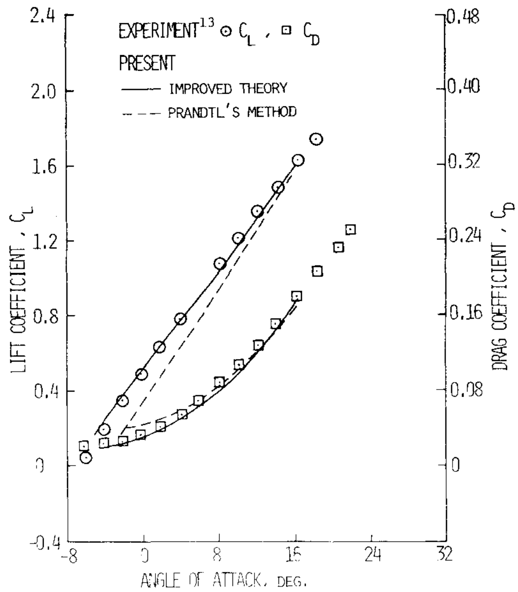

Fig. 2 Comparison of theories with experiment for a wing with partial-span flap: 50% inboard flap span, $AR=6$, $\lambda=0.5$, $\Lambda_{c/4}=9.67$ deg, $M_\infty=0$, and $N=40$.

comparison of the theories for a wing of $AR=6$ with 50% inboard flap span. The flapped section data are given in Ref. 13 and the clean section data are taken from Ref. 12. Again, the present improved method predicts results in good agreement with experiment. Prandtl's method is seen to produce lower lift in this case. Examination of the numerical results indicates that while Prandtl's theory produces slightly lower downwash over the flapped span, it gives much lower upwash over the outboard clean span which is due to the strong trailing vortices from the inboard flapped section. This is probably the aspect-ratio effect, because as the aspect ratio is increased to 10, Prandtl's theory predicted higher lift.

Concluding Remarks

An improved nonlinear lifting-line theory has been presented with applications. The new theory, which allows the use of nonlinear section data, predicts aerodynamic characteristics of wings of moderate to high aspect ratios with or without sweep in better agreement with experiment than Prandtl's theory. The theory can be used to convert the airfoil characteristics to wing characteristics.

Acknowledgment

This investigation was supported by University of Kansas General Research allocation No. 3839-5038.

References

[1]Sivells, J. C. and Neely, R. H., "Method for Calculating Wing Characteristics by Lifting-Line Theory Using Nonlinear Section Lift Data," NACA Rept. 865, 1947.

[2]Sivells, J. C. and Westrick, G. C., "Method for Calculating Lift Distributions for Unswept Wings with Flaps or Ailerons by Use of Nonlinear Section Lift Data," NACA Rept. 1090, 1952.

[3]McVeigh, M. A. and Kisielowski, E., "A Design Summary of Stall Characteristics of Straight Wing Aircraft," NASA CR-1646, 1971.

[4]Smetana, F.O., Summey, D.C., Smith, N.S., and Carden, R. K., "Light Aircraft Lift, Drag and Moment Prediction – A Review and Analysis," NASA CR-2523, 1975.

[5]Weissinger, J., "The Lift Distribution of Swept-Back Wings," NACA TM 1120, 1947.

[6]Lan, C., "An Improved Nonlinear Lifting-Line Theory," *AIAA Journal*, Vol. 11, May 1973, pp. 739-742.

[7]Fasce, M. H., "Applications of an Improved Nonlinear Lifting-Line Theory," M. S. Thesis, Department of Aerospace Engineering, University of Kansas, March 1975.

[8]Lan, C. E., "A Quasi-Vortex-Lattice Method in Thin Wing Therory," *Journal of Aircraft*, Vol. 11, Sept. 1974, pp. 518-527.

[9]Multhopp, H., "Methods for Calculating the Lift Distribution of Wings (Subsonic Lifting-Surface Theory)," British ARC R&M 2884, 1950.

[10]Weber, J., "The Calculation of the Pressure Distribution over the Surface of Two-Dimensional and Swept Wings with Symmetrical Aerofoil Sections," British ARC, R&M 2918, 1953.

[11]Anderson, R. F., "Determination of the Characteristics of Tapered Wings," NACA Rept. 572, 1936.

[12]Abbot, I. H. and Von Doenhoff, A. E., *Theory of Wing Sections*, Dover, New York, 1959.

[13]Pearson, H. A. and Anderson, R. F., "Calculation of the Aerodynamic Characteristics of Tapered Wings with Partial-Span Flaps," NACA Rept. 665, 1939.

Prediction of Tethered-Aerostat Response to Atmospheric Turbulence

James DeLaurier*
Institute for Aerospace Studies, University of Toronto, Toronto, Canada

Introduction

WITHIN recent years, aerodynamically shaped tethered balloons (aerostats) have been used as "skyhooks" and instrument-carrying elevated platforms. For example, the skyhook applications have included balloon logging[1] and experiments in ship-cargo unloading[2]; platform applications include telecommunications relay,[3] optical surveillance,[4] and atmospheric measurements.[5]

For all of these examples, the operational advantages of utilizing an aerostat are compromised by its inherent unsteadiness in atmospheric turbulence. A tethered-aerostat system is useful only if this unsteadiness is small enough to allow it to perform its tasks.

In 1970, DeLaurier[6] developed an analysis by which the first-order station-keeping stability of a tethered aerostat could be predicted. This was applied to the configuration design of the Family-II aerostat (Fig. 1), and experiments confirmed the theoretical predictions of first-order stability throughout its flight envelope.[7] However, first-order stability only guarantees steadiness in steady winds. Although it is a necessary condition for minimal response to turbulence, it is not sufficient.

In order to address this problem, DeLaurier[8] developed an analysis by which the rms lateral response of a tethered aerostat may be predicted. This Note describes the development of a corresponding longitudinal analysis, and the application of both analyses to an example Family-II aerostat.

Method of Analysis

The spectral approach was used for this work, where the cable-aerostat system's transfer functions to a spectral component of turbulence were combined with an atmospheric-turbulence power-spectrum function to obtain power functions of the system's responses. Then, by integration, mean square values for the responses were obtained. This is analogous to the aircraft turbulence-response analysis described by Etkin,[9] where turbulence was considered to be "frozen" with respect to the atmosphere, and the vehicle was excited by flying through it.

Received Oct. 26, 1976.

Index categories: Aircraft Gust Loading and Wind Shear; Aircraft Handling, Stability, and Control; Aircraft Performance.

*Associate Professor.

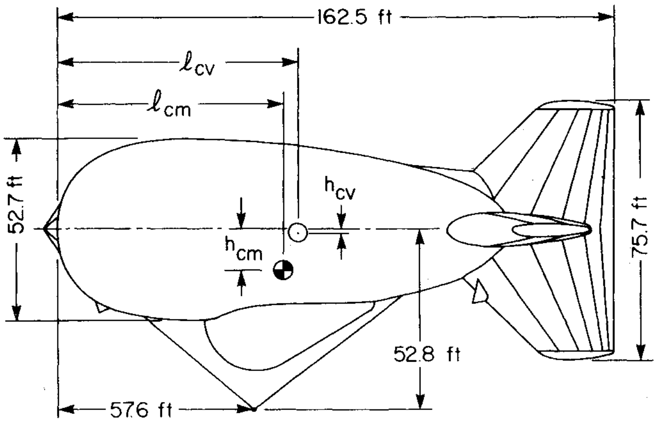

Fig. 1 Side view of the SN 204 Family-II aerostat.

For this case, the "frozen-field" assumption is again used, with the conceptual change that the vehicle is excited by the field passing around it at a mean wind speed U_0. Therefore, for aerostats whose lateral dimensions are small compared with their longitudinal dimensions, the turbulence field within the region of the aerostat, and with respect to its mass center, is given by

$$u_g = CU_0 \exp(i\omega t) \tag{1}$$

$$v_g = BU_0 \exp(i\omega t) \exp(i\omega x/U_0) \tag{2}$$

$$w_g = AU_0 \exp(i\omega t) \exp(i\omega x/U_0) \tag{3}$$

where x, y, z are the traditional body-fixed wind axes[10]; u_g, v_g, w_g are the turbulence-spectrum velocity components in the negative x, y, and z directions, respectively; A, B, C are magnitudes of the components; t is time; and ω is the spectrum frequency, which is given by

$$\omega = -2\pi U_0/\lambda \tag{4}$$

where λ is the spectrum wavelength.

Furthermore, the "long-wavelength" assumption[9] was applied, where it is assumed that the most energetic spectrum wavelengths are at least eight times longer than the length of the vehicle. This means that the axial variations of v_g and w_g are nearly linear within the length of the aerostat, and that the turbulent forcing may be obtained by using the vehicle's stability derivatives. For example, the w_g excitation is given by

$$X_g = X_\alpha \alpha_g + X_{\dot\alpha}\dot\alpha_g + X_q q_g + X_{\dot q}\dot q_g \tag{5}$$

$$Z_g = Z_\alpha \alpha_g + Z_{\dot\alpha}\dot\alpha_g + Z_q q_g + Z_{\dot q}\dot q_g \tag{6}$$

$$M_g = M_\alpha \alpha_g + M_{\dot\alpha}\dot\alpha_g + M_q q_g + M_{\dot q}\dot q_g \tag{7}$$

where X_g, Z_g are the turbulence forces in the x and z directions, respectively; M_g is the turbulence moment about the y axis; X_α, $X_{\dot\alpha}$, Z_q, $M_{\dot q}$, etc. are the dimensional stability derivatives[10]; and

$$\alpha_g = A \exp(i\omega t) \tag{8}$$

$$q_g = -i\omega A \exp(i\omega t) \tag{9}$$

$$\dot\alpha_g = i\omega A \exp(i\omega t) \tag{10}$$

$$\dot q_g = \omega^2 A \exp(i\omega t) \tag{11}$$

Similarly, equations for the u_g and v_g excitation were obtained. These were then nondimensionalized and added to the nondimensional first-order unforced cable-aerostat dynamic equations of Refs. 6 and 7. For this case, the cable's dynamics were ignored, and it was thus modelled by a massless, dragless rod. The particular solutions of the resulting equations gave the system's transfer functions which, for the w_g excitation, had the form

$$x/\alpha_g = |x/\alpha_g| \exp(i\omega t)\exp(i\delta_x) \tag{12}$$

$$\theta/\alpha_g = |\theta/\alpha_g| \exp(i\omega t)\exp(i\delta_\theta) \tag{13}$$

$$\Delta T/\alpha_g = |\Delta T/\alpha_g| \exp(i\omega t)\exp(i\delta_T) \tag{14}$$

where x is the change in aerostat axial displacement; θ is the change in aerostat pitch angle; ΔT is the change in tether tension; and δ_x, δ_θ, δ_T are the phase angles for the x, θ, and ΔT variations with respect to α_g.

Note that the transfer functions are uncoupled between longitudinal and lateral responses, where the total longitudinal response is due both to u_g and w_g excitation, and the lateral response is due solely to v_g. Furthermore, the lateral solution, as described in Ref. 8, gives values for the lateral displacement variation y, the change in heading angle ψ, and the roll angle ϕ.

The power functions for the dynamic response to turbulence were obtained from the magnitudes of the transfer functions and power functions for the atmosphere's turbulence components $P_u(\omega)$, $P_v(\omega)$, and $P_w(\omega)$. For example, the longitudinal functions are

$$P_x(\omega) = |x/u_g|^2 P_u(\omega) + |x/\alpha_g|^2 P_w(\omega)/U_0^2 \tag{15}$$

$$P_\theta(\omega) = |\theta/u_g|^2 P_u(\omega) + |\theta/\alpha_g|^2 P_w(\omega)/U_0^2 \tag{16}$$

$$P_T(\omega) = |\Delta T/u_g|^2 P_u(\omega) + |\Delta T/\alpha_g|^2 P_w(\omega)/U_0^2 \tag{17}$$

Finally, the rms values for the responses were obtained from the square roots of the power-function integrals. For example

$$x_{rms} = \left[\int_0^\infty P_x(\omega)\,d\omega\right]^{1/2} \tag{18}$$

$$\theta_{rms} = \left[\int_0^\infty P_\theta(\omega)\,d\omega\right]^{1/2} \tag{19}$$

$$\Delta T_{rms} = \left[\int_0^\infty P_T(\omega)\,d\omega\right]^{1/2} \tag{20}$$

where

$$(u_g)_{rms} = \left[\int_0^\infty P_u(\omega)\,d\omega\right]^{1/2} \tag{21}$$

$$(w_g)_{rms} = \left[\int_0^\infty P_w(\omega)\,d\omega\right]^{1/2} \tag{22}$$

Numerical Example

The analysis was applied to SN 204 of the Family-II series of aerostats, whose physical characteristics are given in Ref. 7. Also, the atmospheric-turbulence power functions were obtained from Teunissen[11] who uses the von Karman model along with equations and graphs for the intensities, $\bar u_g^2$, $\bar v_g^2$, $\bar w_g^2$, and scale lengths, Lx, Ly, Lz. For this particular case, the cable length is 1000 ft and is tethered at sea level on smooth terrain. From Ref. 11, this gives

$$\bar u_g^2 = \bar v_g^2 = \bar w_g^2 = 0.0004U_0^2 \tag{23}$$

$$Lx = 650\text{ ft} \qquad Ly = Lz = 325\text{ ft} \tag{24}$$

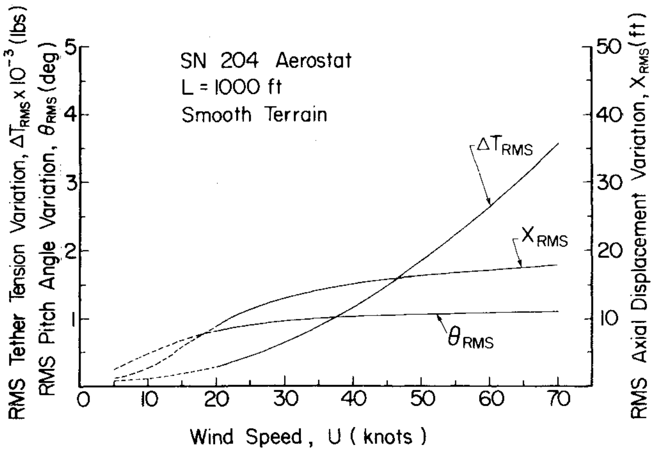

Fig. 2 Predicted rms longitudinal response to atmospheric turbulence.

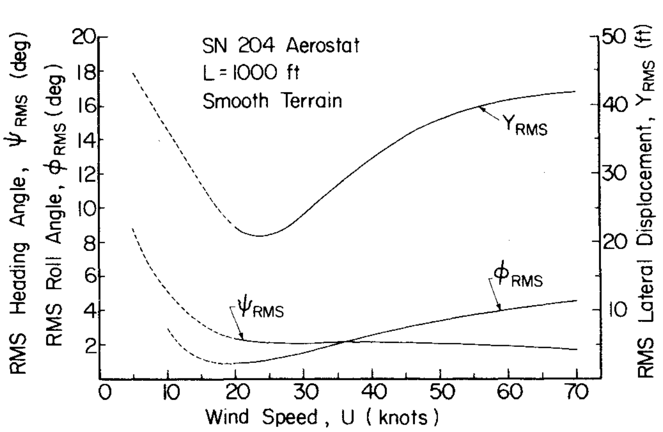

Fig. 3 Predicted rms lateral response to atmospheric turbulence.

and the resulting responses for a wind-speed range of 5 to 70 knots are given in Figs. 2 and 3. Note that the long-wavelength assumption is violated at U_0 below 20 knots. Therefore the dashed portions of the curves are only qualitative variations.

Upon comparison of Figs. 2 and 3, one sees that lateral displacement, y_{rms}, is generally twice the magnitude of the axial displacement, x_{rms}; similarly, the heading angle, ψ_{rms}, is approximately twice as sensitive to turbulence as the pitch angle variation, θ_{rms}. This behavior was qualitatively observed during the SN 204's flight tests. Furthermore, the w_g excitation was over twice as effective as u_g for producing axial responses, and was nearly 10 times as effective in producing pitch responses. Finally, it was found that ΔT_{rms} was due primarily to $\Delta\theta_{rms}$ so that

$$\Delta T_{rms} \cong \frac{\rho U_0^2 S}{2} C_{L_\alpha} \Delta\theta_{rms} \tag{25}$$

Note the alarming increase in ΔT_{rms} with U_0, even for this "smooth-terrain" case. It is clear that configuration redesign to lower θ_{rms} would reduce the required cable safety factor, and hence its weight and drag.

Concluding Remarks

The most important restrictions on the physical model are the long-wavelength assumption and the massless, dragless cable assumption. For aerostats the size of the SN 204, these constrain the validity of this analysis to wind speeds above 20 knots and cable lengths less than 1500 ft. Within this envelope, however, the physical model is well justified, and the analysis should predict an aerostat's behavior with reasonable accuracy.

Currently, this analysis is being used to develop aerostat configurations that will have minimum response to turbulence and hence maximum station-keeping ability. The results from this work will be the subject of a future report.

References

[1]Garlicki, A. and Richenhaller, J., "Logging with Balloons and Helicopters – An Annotated Bibliography," Forest Management Service, Ottawa, Ontario, Canada, Information Report FMR-X-69, Feb. 1975.

[2]Reed, H.E., "A Balloon Transport System," AIAA Paper 75-926, *AIAA Lighter-than-Air Technology Conference,* Snowmass, Colorado, July 15-17, 1975.

[3]Anon., "Tethered Balloon Used for Signal Relay," *Aviation Week and Space Technology,* Vol. 100, April 29, 1974, pp. 52-53.

[4]McLaren, E.J., private communication, Canada Centre for Remote Sensing, Ottawa, Canada, Sept. 1976.

[5]Mickle, R.E. and Davison, D.F., "Results from Sea Trials of a New Boundary-Layer Tethersonde Package," presented at the *Eighth Annual Congress of the Canadian Meteorological Society,* Toronto, Canada, May 30, 1974.

[6]DeLaurier, J.D., "A Stability Analysis for Tethered Aerodynamically Shaped Balloons," *Journal of Aircraft,* Vol. 9, Sept. 1972, pp. 646-651.

[7]DeLaurier, J.D., "Refinements and Experimental Comparisons of a Stability Analysis for Aerodynamically-Shaped Tethered Balloons," AIAA Paper 75-943, *AIAA Lighter-than-Air Technology Conference,* Snowmass, Colorado, July 15-17, 1975.

[8]DeLaurier, J.D., "An Analytical Method for Predicting a Tethered Aerostat's Lateral Response to Atmospheric Turbulence," *Proceedings Ninth AFGL Scientific Balloon Symposium,* Air Force Geophysics Laboratory, Oct. 1976.

[9]Etkin, B., "Flight in Turbulent Air," *Dynamics of Flight,* Wiley, New York, 1966, pp. 310-340.

[10]Ashley, H., "Small Perturbation Response and Dynamic Stability of Flight Vehicles," *Engineering Analysis of Flight Vehicles,* Addison-Wesley, Menlo Park, Calif. 1974, pp. 173-202.

[11]Teunissen, H.W., "Characteristics of the Mean Wind and Turbulence in the Planetary Boundary Layer," UTIAS Review No. 32, Oct., 1970, University of Toronto's Institute for Aerospace Studies, Downsview, Ontario.

Thrust Augmenting Ejector Analogy

Hermann Viets*
Wright State University, Dayton, Ohio

THRUST augmentation sometimes has been viewed by those not directly involved as a violation of basic principles, i.e., something for nothing. This is probably because the total momentum at the ejector exit is greater than the input momentum, a situation which is intuitively disquieting. It is the purpose of this Note to illustrate the same effect in terms of colliding railroad cars and thereby to put thrust augmentation and some of the attendant details on a more intuitive footing. This is a timely objective since a prototype aircraft employing thrust augmentation is currently under construction by Rockwell International for the U.S. Navy.

A schematic of a thrust augmenting ejector is shown in Fig. 1. The primary nozzle is placed within the ejector shroud and expells high-pressure air. The mixing of the surrounding air with the primary air causes a low-pressure region downstream of the nozzle exit which causes ambient air to be entrained into the ejector. The primary and entrained flows are mixed

Received June 25, 1976; revision received Oct. 25, 1976.

Index catagories: Airbreathing Propulsion, Subsonic and Supersonic; Nozzle and Channel Flow; VTOL Powerplant Design and Installation.

*Associate Professor. Associate Fellow AIAA.